JOURNAL OF SOLID STATE CHEMISTRY 101, 296–308 (1992)

Ordered Magnetic Frustration: XVII. Is $BaMnFeF_7$ Frustrated? Mössbauer Spectroscopy, Magnetic Susceptibility, and Magnetic Structure at 2 K

P. LACORRE* AND J. PANNETIER

Institut Laue Langevin, 156X, Avenue des Martyrs, 38042 Grenoble Cedex, France

J. PEBLER, S. NAGEL, AND D. BABEL

Fachbereich Chemie und Wissenschaftliches Zentrum für Materialwissenschaften der Philipps-Universität, Hans-Meerwein-Strasse, D-3550 Marburg, Federal Republic of Germany

A. DE KOZAK AND M. SAMOUËL

Laboratoire de Cristallochimie du Solide, U.R.A. C.N.R.S. 1388, Université P. et M. Curie, Tour 54, 4, Place Jussieu, 75252 Paris Cedex 05, France

AND G. FÉREY

Laboratoire des Fluorures, U.R.A. C.N.R.S. 449, Université du Maine, Avenue Olivier Messiaen, 72017 Le Mans Cedex, France

Received January 29, 1992; accepted May 7, 1992

The results of a series of magnetic measurements on the fluoride $BaMnFeF_7$, including magnetic susceptibility, Mössbauer spectra, and neutron powder diffraction, are presented. The compound orders antiferromagnetically below $T_N = 84.9(5)$ K and its paramagnetic Curie temperature is $\theta_P = -217(5)$ K. The Mössbauer parameters are in good agreement with those of other iron(III) fluorides. The magnetic structure determined by neutron diffraction ($R_{mag} = 0.052$) shows that the spin sublattices of Mn and Fe each are ferromagnetic and mutually are coupled antiferromagnetically. The magnetic moments lie in the (**a**,**c**) plane, mainly oriented along the **c** direction. The presence of magnetic frustration in the compound depends on the sign of the 90° exchange interaction Mn–F–Mn. Whatever this sign may be, the weakness of this interaction guarantees the consistency of the magnetic structure with the known d^5–d^5 coupling mechanisms.

1. Introduction

In the previous papers of this series (*1–16*), various fluorides undergoing topological ordered magnetic frustration have been studied. In most cases, frustration (*17, 18*) arises from antiferromagnetic interactions within triangular platelets (triangular cycles) of 3-D cations inside corner-sharing coordination octahedra. Sometimes, the presence of both corner-sharing and edge-sharing coordination octahedra can also

* To whom correspondence should be addressed at present address: Laboratoire des Fluorures, U.R.A. C.N.R.S. 449, Université du Maine, Avenue Olivier Messiaen, 72017 Le Mans Cedex, France.

0022-4596/92 $5.00

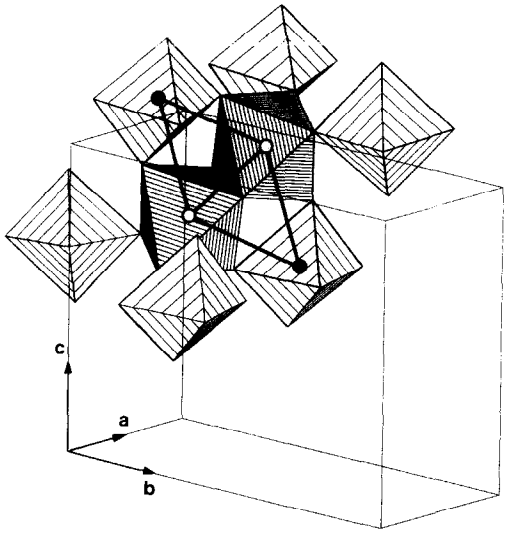

FIG. 1. Triangular platelets of magnetic cations in $BaMnFeF_7$. Mn^{2+} cations (open circles) and Fe^{3+} cations (closed circles) are located in heavily and lightly hatched coordination octahedra, respectively.

lead to frustrated spin arrangements as in $Ba_2Ni_3F_{10}$ (*9*). $BaMnFeF_7$ (*19, 20*), the crystal structure of which has recently been solved by three of us (*21*), provides another example where these two configurations occur, both combining to yield triangular platelets of magnetic cations (see Fig. 1).

In this paper we present the results of Mössbauer and bulk magnetic susceptibility measurements (Section 3), as well as the crystal and the magnetic structure of $BaMnFeF_7$, as determined by neutron powder diffraction (Section 4). Finally, the exchange interactions and the possible presence of magnetic frustration in this compound are discussed (Section 5).

2. Experimental

Sample preparation. The samples used for the various measurements have been prepared according to the procedure presented previously (*19*).

Mössbauer spectroscopy. The experiments were performed on a powder sample with 8 mg natural Fe per square centimeter absorber surface. Mössbauer spectra were recorded in transmission geometry applying usual techniques. A 25-mCi source of ^{57}Co in palladium was used as a reference. The calibration was effected with a metallic-iron absorber. All velocity scales and isomer shifts were referred to the Co(Pd) source at room temperature and converted to the iron standard at 295 K by adding 0.185 mm/sec. The measurements were performed from 4.2 to 300 K using a vacuum cryofurnace. The absorber temperature accuracy was about 0.5 K while the temperature stability was better than 0.2 K.

Prior to data analysis, the independent spectra obtained in the two analyzer halves were combined to eliminate geometric distortion. Least-squares fits were then made using symmetrical Lorentzian lines, specified by position, width, and amplitude.

Magnetization and magnetic susceptibility. Magnetization and susceptibility were measured on powdered samples by means of a Foner-type vibrating sample magnetometer (4.2 K $< T <$ 90 K) and a Faraday balance (90 K $< T <$ 300 K), respectively. Corrections for the diamagnetic ionic contributions were applied. The temperature stability of the cryostats used was better than 0.3 K. Above 90 K, all measurements were performed at three different field strengths (1 kG $< H <$ 5 kG) and no field dependence of the magnetic susceptibilities was observed. Below 90 K, the magnetic susceptibility was calculated from the magnetization measured as a function of applied fields (up to 20 kG).

Neutron scattering. Preliminary measurements were done on the high flux powder diffractometer D1B of the Institut Laue Langevin (ILL) in Grenoble. For the structure refinements, two neutron diffraction patterns were collected at 2 and 116 K on the powder diffractometer D1A of the ILL. For current experiments, the wavelength was fixed to 1.909 Å. The full angular range

($0° < 2\theta < 160°$) was scanned by steps of 0.05°.

The powder sample was contained in a vanadium cylinder (ϕ = 15 mm). For the low temperature measurements, the container was placed in a liquid helium cryostat with programmable temperature (1.5 K < T < 300 K) and stability better than 0.1 K.

The structural refinements were performed by fitting the whole observed profile to a calculated profile of Gaussian peaks, according to the method introduced by Rietveld (*22*) and modified by Hewat (*23*). The nuclear scattering lengths and magnetic form factors were taken from Koester and Rauch (*24*) and Watson and Freeman (*25*), respectively. To specify the possible models of magnetic structure, Bertaut's macroscopic theory was used (*26*).

3. Bulk Magnetic Measurements

Mössbauer effect. The Mössbauer spectra of $BaMnFeF_7$ at several temperatures are shown in Fig. 2. In each spectrum there is evidence for a small amount of paramag-

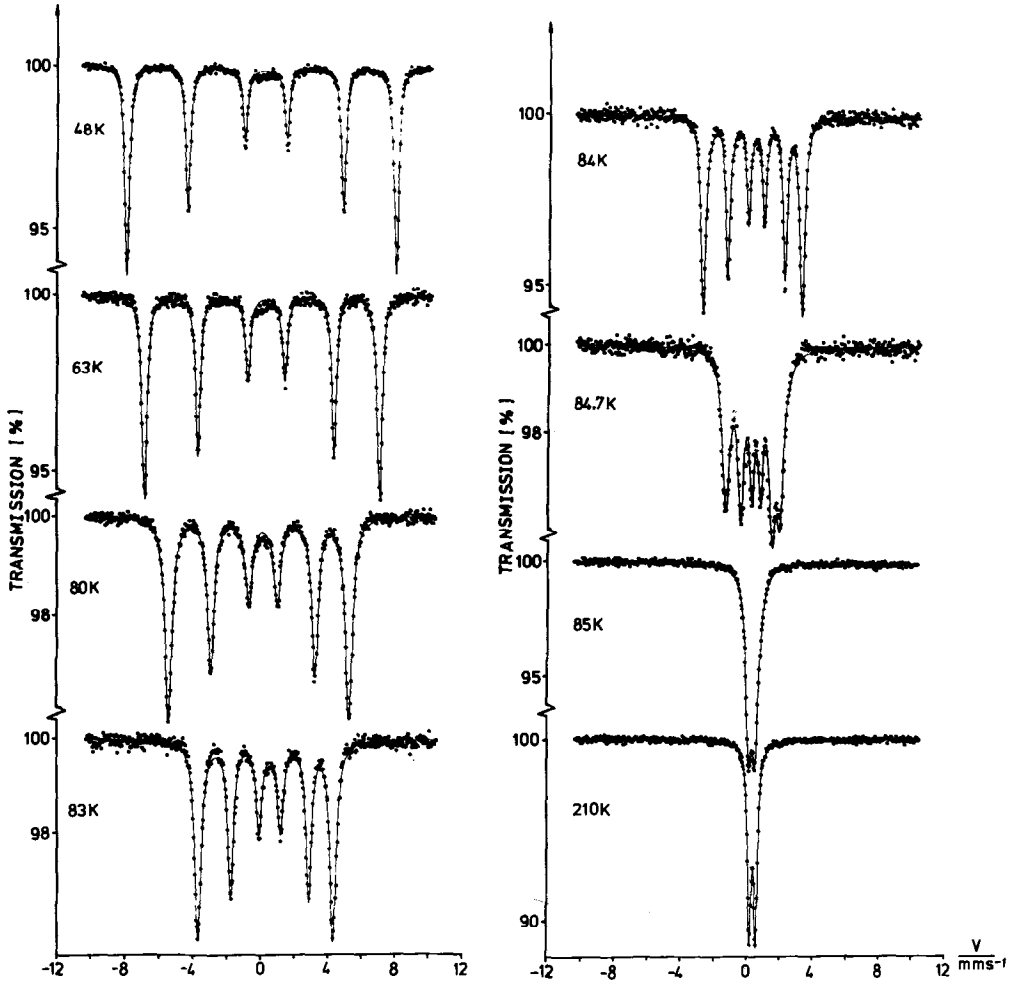

FIG. 2. Least-squares fits to the Mössbauer absorption spectra of $BaMnFeF_7$ below and above the Néel temperature T_N = 84.9 K.

TABLE I

SUMMARY OF THE MÖSSBAUER DATA: MAGNETIC HYPERFINE FIELD, H; ISOMER SHIFT, IS; QUADRUPOLE SPLITTING, EQ (SHIFT BELOW T_N); MEAN LINEWIDTH, W; AND AREA RATIOS OF THE ABSORPTION LINES BELOW T_N AT SELECTED TEMPERATURES

T (K)	H (kOe)	IS (mm/sec)	EQ (mm/sec)	W (mm/sec)	Area ratios
4.2	579(3)	0.524(7)	−0.108(5)	0.33(1)	2.83 : 2.05 : 1.12
11.0	575(3)	0.523(7)	−0.107(5)	0.33(1)	2.83 : 2.05 : 1.12
48.0	495(3)	0.560(7)	−0.109(5)	0.33(1)	2.83 : 2.05 : 1.12
63.0	432(3)	0.555(7)	−0.110(5)	0.33(1)	2.83 : 2.05 : 1.12
80.0	296(3)	0.552(7)	−0.111(5)	0.34(1)	2.84 : 2.00 : 1.16
84.7	100(3)	0.546(8)	−0.105(5)	0.46(2)	2.69 : 2.03 : 1.28
85.0	—	0.548(3)	0.400(3)	0.40(2)	—
90.0	—	0.545(3)	0.395(3)	0.34(2)	—
145.0	—	0.514(5)	0.372(3)	0.32(2)	—
210.0	—	0.485(3)	0.369(3)	0.32(2)	—

Note. The temperatures were stable to +/−0.2 K. The isomer-shift values are given relative to iron metal at room temperature.

netic impurity. This impurity becomes apparent, for example, in the center of the 63-K spectrum. The Mössbauer effect parameters derived from the calculated fits to the spectra are given in Table I; the fitted curves are represented by the solid lines in Fig. 2. The results indicate that $BaMnFeF_7$ is paramagnetic above 85 K. The typical values of the chemical shifts and quadrupole splittings confirm the paramagnetic high spin Fe^{3+} ion to be within an essentially octahedral crystal field. The room temperature isomer shift of 0.430 mm/sec is in good agreement with the observed value of 0.485 mm/sec for rhombohedral FeF_3 (*27, 28*). As expected for the ${}^6A_{1g}$ electronic state, the quadrupole interaction does not change very much with temperature. The larger linewidths just above 85 K probably result from the impending magnetic ordering which occurs near 84.9 K. Below $T_N = 85$ K the magnetic hyperfine field increase with decreasing temperature follows a Brillouin function (see Fig. 3). The Mössbauer spectra in this region consist of typical six-line magnetic splittings which become most pronounced at the lowest temperatures. The deviation from the theoretical area ratio 3 : 2 : 1 (see Table I) may be attributed to the saturation effect caused by the thickness of the absorber. The field of 579 kOe at 4.2 K is close to saturation, but has a lower value than the 625 kOe predicted for Fermi contact interaction of a free $3d^5$ system and nearly found so in FeF_3 (*27*). Experiments in high fields up to 60 kG have shown $BaMnFeF_7$ to behave as a simple hard antiferromagnet (*29*).

The hyperfine field curve in Fig. 3 cuts the temperature axis at 84.9 K and is essentially perpendicular to it when approaching zero field. This indicates a very sharp Néel point and transition into a three-dimensionally ordered phase. The line intensities have been normalized to add up to 6 (Table I). There is little change in these relative intensities, except when approaching the Néel temperature. Within 1 K near this point the outer lines lose 10% in intensity and increase in linewidth by 50%. These asymmetrical line shapes are a consequence of the nonlinear change of magnetization with temperature near the critical point. However, we did not find any temperature range in which magnetically ordered and paramagnetic material coexist.

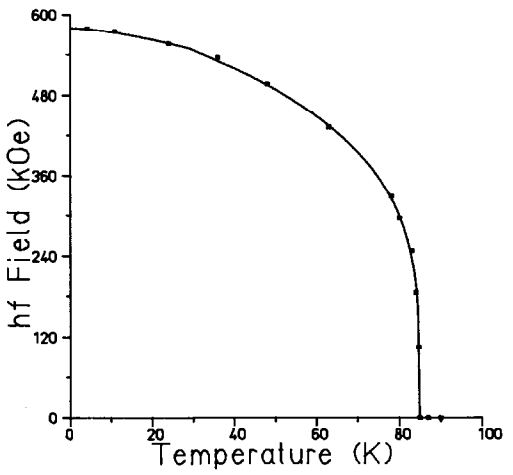

FIG. 3. The hyperfine effective field as a function of temperature.

The solid line in Fig. 3 represents least-squares fits of the magnetic hyperfine field values to the spin waves law $H(T) = H_0(1 - A * T^{3/2})$ below 40 K (with $A = 3.5 \times 10^{-4}$ K$^{-3/2}$) and to the critical law $H(T) = D * H_0 * (1 - T/T_N)^{\beta}$ above this temperature. The critical parameters ($H_0 = 579$ kOe, $T_N = 84.9$ K, $D = 1.05$, and $\beta = 0.25$) are in good agreement with those reported from other fluorides (*30*). It is worth mentioning that the saturation field of $H_0 = 579(3)$ kOe and the transition temperature of $T_N = 84.9(5)$ K in $BaMnFeF_7$ do not differ very much from the observations in the related compounds Na_2MnFeF_7 ($H_{01} = 554(5)$ kOe, $H_{02} = 544(5)$ kOe; $T_N = 94(1)$ K) (*31*) and Na_2NiFeF_7 ($H_0 = 543(3)$ kOe; $T_N = 88.4(8)$ K). The approximate conformity of the Néel temperatures seems to indicate that, in spite of all structural differences, the exchange interactions are very similar in these three compounds.

The linewidths of the Mössbauer spectra are, except at the magnetic transition, close to the expected residual linewidth of 0.32 mm/sec, indicating that the spin relaxation time is sufficiently short, i.e., much shorter than the Larmor period, so that a true time-average field exists at the nucleus. Thus in $BaMnFeF_7$, the magnetic hyperfine field should be proportional to the sublattice magnetization. Therefore, in connection with the determination of the magnetic structure of the compound, we calculated the relative orientation of the magnetic hyperfine field in the crystal axis system. The Mössbauer spectra have been fitted with the parameters $\vartheta = 20(5)°$, $\varphi = +/-80°$, and $\eta = 0.2$, where η is the asymmetry parameter, and ϑ and φ describe the direction of H relative to the main component of the electric field gradient (e.f.g.) tensor V_{zz}.

The sign of the quadrupole coupling constant and the orientation of V_{zz} could not be determined experimentally. However, it is possible to obtain this information by theoretical methods. Within a simple model and considering the ions as point charges, the e.f.g. tensor is calculated from lattice sums. Using formal charges one obtains ${}^{ion}V_{zz} = -0.0516e/a_{H^3}$ and $\eta = 0.53$, where a_H denotes the Bohr radius (*32*). The orientation of the principal axes (X,Y,Z) of the e.f.g. tensor depends on the equivalent position considered. For Fe at (0.69, 0.12, 0.77) the Z axis of the tensor forms angles of 71°, 126°, and 45° with the **a**, **b**, and **c** crystal axes, respectively. Within the ionic model, the asymmetry parameter and the orientation of the principal axes are independent of the antishielding effect which amplifies ${}^{ion}V_{zz}$ by $V_{zz} = (1 - \gamma_\infty){}^{ion}V_{zz}$ with $\gamma_\infty \approx -9$ for Fe^{3+} (*32*). Thus the ionic model predicts a negative quadrupole coupling constant $eQV_{zz}/2$. For a nuclear quadrupole moment of 0.1 b, the quadrupole splitting in mm/sec is obtained by multiplying $V_{zz}(e/a_{H^3})$ by a factor of about 1. Thus the calculated quadrupole splitting is about -0.5 mm/sec, in fair agreement with experiment.

In order to consider a possible influence of chemical bonding on the e.f.g., spin-polarized all-electron cluster calculations (*33*) have also been performed. This approach allows the calculation of hyperfine parame-

ters from the electronic wave functions. The first coordination shell of Fe^{3+} has been considered, with positional parameters taken from the refinement of Holler *et al.* (*21*).

The e.f.g. is calculated from $V_{ij} = {}^{Fe}V_{ij}$, where ${}^{Fe}V_{ij}$ is the contribution due to the deformation of the iron charge. Diagonalization gives $V_{zz} = -19e/a_{H^3}$, corresponding to about -0.2 mm/sec and $\eta = 1$. The orientation of the principal axes is very similar to that obtained from the ionic model discussed above. The calculated values turn out to be slightly dependent on the way the cluster is embedded in the crystal potential; however, the results confirm a negative sign of the quadrupole constant.

Based on the calculated principal axes system and on the relative orientation of the magnetic hyperfine field obtained from the Mössbauer spectra, it is possible to derive the direction of the magnetic field in the crystal axes system. Considering a possible ambiguity of $\varphi = +/-80°$, we end up with two solutions:

1. $\mathbf{H}_1/H_1 = (0.44, -0.75, 0.49)$
2. $\mathbf{H}_2/H_2 = (0.27, -0.26, 0.93)$.

Solution 2 was found to be in very good agreement with the neutron diffraction results given below.

Magnetic susceptibility. The inverse molar magnetic susceptibility of $BaMnFeF_7$ is plotted vs temperature in Fig. 4. All values above 90 K are field-weighted averages of measurements at three different fields. The susceptibilities below 90 K were calculated from the slopes of magnetization plots vs applied field. The magnetization increase was linear. However, below the $1/\chi$ minimum at 85 K, which marks the transition to the three-dimensionally ordered state, extrapolation to zero field yields small positive values, indicating spontaneous magnetization.

The linear part of the $1/\chi$ plot vs temperature can be extrapolated to a large negative Curie–Weiss temperature θ_P. Using only

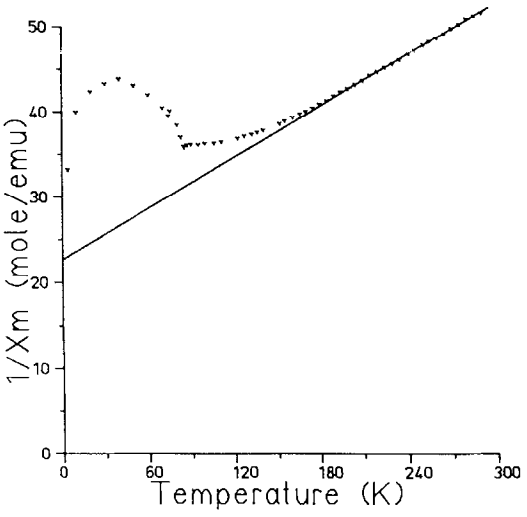

FIG. 4. Plot of the reciprocal molar magnetic susceptibility of $BaMnFeF_7$ as a function of temperature. The extrapolated least-squares line through the experimental values is based on the data obtained above 200 K and gives a θ_P value of -217 K.

data above 200 K in a linear least-squares extrapolation to $1/\chi = 0$, the value obtained is $\theta_P = -217(5)$ K, a figure well comparable with that of related antiferromagnetic materials. Application of the Curie–Weiss law with temperatures corrected by $\theta_P = -217$ K yields a magnetic moment of 6.2 μB, close to the spin-only moment of 5.9 μB for the isoelectronic d^5 cations Mn^{2+} and Fe^{3+}.

Below T_N, the temperature behavior of the $1/\chi$ curve is anomalous. There is a strong indication either of some ferromagnetic impurity within the sample (but also present in different preparations) or of an unusual (e.g., varying) spin canting of the material itself, exhibiting a maximum at about 70 K. Neutron diffraction measurements performed near this temperature did not give any support to the latter interpretation.

4. Crystal and Magnetic Structures at 2 K

$BaMnFeF_7$ crystallizes in the monoclinic space group $P2_1/c$ with room temperature

cell parameters $a = 5.532(1)$ Å, $b = 10.980(2)$ Å, $c = 9.183(1)$ Å, $\beta = 94.67(1)°$ ($Z = 4$) (*21*). All atoms occupy general positions 4*e* of the space group. As mentioned in the previous section, susceptibility measurements (Fig. 4) suggest three-dimensional antiferromagnetic ordering below 85 K; the remanent magnetization, if any, must be very small at low temperature. At 2 K a low temperature neutron diffraction pattern has been recorded. Compared to a pattern at higher temperature ($T = 116$ K), it shows a large enhancement of several nuclear peaks, but no additional lines. Thus the magnetic cell is equal to the crystal cell.

The possible coupling modes of the magnetic moments in $BaMnFeF_7$ have been determined using Bertaut's macroscopic theory (*26*). The 2_{1y} screw axis and the inversion center were chosen as independent symmetry elements of the space group $P2_1/c$. The magnetic moments corresponding to four 3*d* cations on equivalent positions are labeled as follows:

$$S_1 \text{ on } x, y, z$$
$$S_2 \text{ on } -x, \tfrac{1}{2} + y, \tfrac{1}{2} - z$$
$$S_3 \text{ on } -x, -y, -z$$
$$S_4 \text{ on } x, \tfrac{1}{2} - y, \tfrac{1}{2} + z.$$

The four base vectors which represent the possible magnetic modes of coupling are expressed, according to Bertaut's notation:

$$F = S_1 + S_2 + S_3 + S_4$$
$$G = S_1 - S_2 + S_3 - S_4$$
$$C = S_1 + S_2 - S_3 - S_4$$
$$A = S_1 - S_2 - S_3 + S_4.$$

The four irreducible representations allowed by the space group $P2_1/c$ are given in Table II. Two of them (Γ_2 and Γ_4) are purely antiferromagnetic, while the other two (Γ_1 and Γ_3) may be compatible with the bulk magnetic measurements on the compound if one assumes that ferromagnetic components of Mn^{2+} and Fe^{3+} spins are either strictly antiparallel or vanishingly small. All four representations have been tested. Refinements in the representation Γ_3 (*FxGyFz*), corresponding to the magnetic space group $P2_1'/c'$, lead to, by far, the best fit.

TABLE II

THE FOUR IRREDUCIBLE REPRESENTATIONS OF COUPLING MODES IN SPACE GROUP $P2_1/c$

	x	*y*	*z*
Γ_1 (+ +)	*Gx*	*Fy*	*Gz*
Γ_2 (+ −)	*Ax*	*Cy*	*Az*
Γ_3 (− +)	*Fx*	*Gy*	*Fz*
Γ_4 (− −)	*Cx*	*Ay*	*Cz*

A small amount of impurity identified as a few percent of MnF_2 has been detected in the pattern. All magnetic and nuclear peaks of MnF_2 fall in the vicinity of—sometimes strong—reflections of $BaMnFeF_7$. Removal of all corresponding regions from the diagram would have reduced the amount of information significantly and was therefore excluded, the more so, as these impurity peaks, except one, are very weak and have little incidence on the refinement. The strongest impurity peak corresponds to the (100) magnetic reflection of MnF_2 and overlaps the (110) magnetic reflection of $BaMnFeF_7$. As the inclusion of this spurious intensity could induce some bias in the refinement, only in this case the corresponding 2θ range was excluded from the fit. Under these conditions, the best reliability factors were, for a range $10° < 2\theta < 150°$:

$$R_I = 0.048 \ (R_{nuc} = 0.047, R_{mag} = 0.052), \quad R_p = 0.085, R_{wp} = 0.095.$$

The observed, calculated, and observed − calculated profiles are shown in Fig. 5. Table III gives the results of the refinement. The crystal structure is quite in accordance

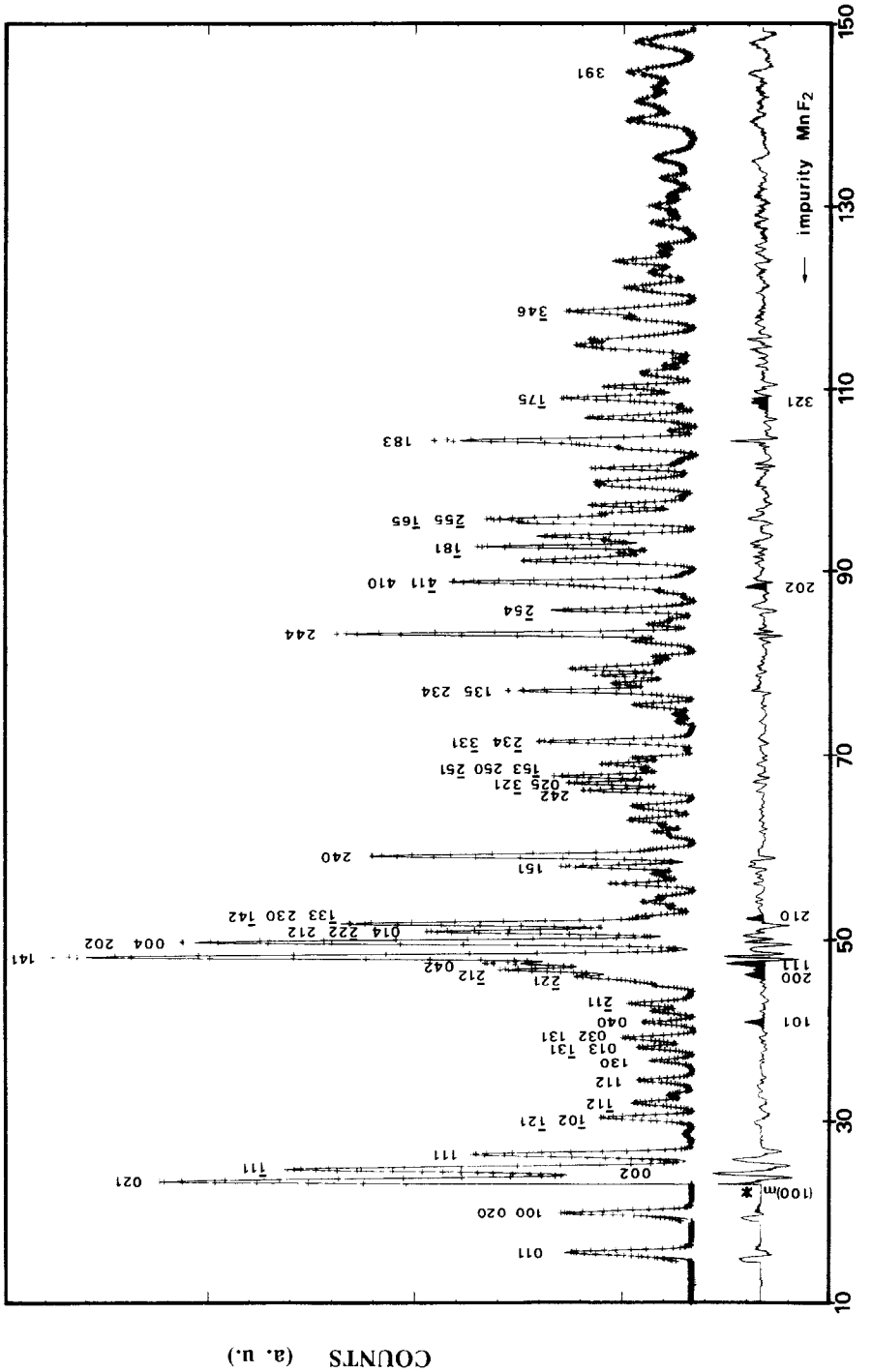

FIG. 5. Observed (+) and calculated (line) neutron diffraction profiles for $BaMnFeF_7$ at 2 K. The difference pattern (observed − calculated) at the same scale is shown on the bottom part of the figure. The parasitic reflections of MnF_2 (bottom) are darkened on the difference pattern. The asterisk indicates the region of the diagram excluded from the refinement.

TABLE III

ATOMIC POSITIONS AND MAGNETIC MOMENTS OF $BaMnFeF_7$ AT 2 K

	Atomic positions				Magnetic moments (μB)			
Atom	*x*	*y*	*z*	*B* (Å^2)	*Mx*	*My*	*Mz*	*M*
Ba	0.2280(9)	0.1685(4)	0.0425(6)	0.64(10)				
Mn	0.8103(10)	0.0631(4)	0.3803(6)	1.20(11)	−0.58(15)	0	−4.09(6)	4.08(6)
Fe	0.6926(4)	0.1205(2)	0.7665(3)	0.94(4)	0.72(14)	0	4.10(7)	4.11(7)
F1	0.4040(10)	0.2823(5)	0.2853(6)	1.32(11)				
F2	0.4993(9)	0.0299(6)	0.2515(4)	0.96(10)				
F3	0.1445(10)	0.3996(4)	0.0107(5)	1.27(11)				
F4	0.9837(8)	0.4835(4)	0.2807(6)	0.80(10)				
F5	0.0972(8)	0.7378(4)	0.2144(5)	0.53(10)				
F6	0.3466(8)	0.6469(4)	0.9398(5)	0.89(11)				
F7	0.7159(10)	0.4053(4)	0.4754(6)	1.27(11)				

Note. Space group $P2_1/c$, a = 5.5075(1) Å, b = 10.9584(2) Å, c = 9.1427(2) Å, β = 94.568(2)°, Z = 4.

with the one previously refined from X-ray single crystal data (*21*), showing only small shifts in atomic coordinates.

The magnetic structure is collinear. The *y* components of the magnetic moments, which always refined to zero within statistical error, were held fixed to this value in final refinements. All Fe^{3+} moments are parallel, and antiparallel to the Mn^{2+} moments (Fig. 6). These moments lie in the (**a,c**) plane, mainly oriented along the **c** axis. As aforesaid, this result removes the uncertainty in the magnetic hyperfine field orientation; it coincides almost exactly with solution 2 given in Section 3. The remanent magnetization, almost negligible when calculated, is consistent with the direct bulk measurements.

Finally, the consistency of the magnetic structure with the expected coupling mechanisms remains to be checked. In a nonfrustrated magnetic structure, the magnetic moments are arranged according to the sign of the interactions. But this is not always true in the case of frustrated structures, as shown in, for instance, $Ba_2Ni_3F_{10}$ (*9*). The presence or absence of magnetic frustration in $BaMnFeF_7$ is not a trivial issue. The collinearity of the magnetic structure is not a sufficient argument against frustration, as previously stressed by the case of $Ba_2Ni_3F_{10}$. The ratio $|\theta_P/T_N|$ is often considered a good experimental indicator of the presence of frustration in a compound (*34*). For a nonfrustrated compound, $|\theta_P/T_N|$ is of the order of unity, while in a frustrated one usually $|\theta_P/T_N|$ is larger than unity (sometimes much larger). The example of the weakly frustrated (*35*) $Ba_2Ni_3F_{10}$ exhibits $|\theta_P/T_N| = 1.4$. The values given in Section 3 yield $|\theta_P/T_N| = 217/85 = 2.55$ for $BaMnFeF_7$, which could

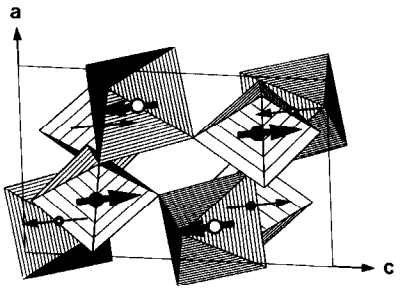

FIG. 6. Magnetic structure of $BaMnFeF_7$. All magnetic moments lie in the (*a,c*) plane of the structure. Open and closed circles represent Mn^{2+} and Fe^{3+} cations, respectively. Thick arrows correspond to magnetic moments carried by atoms in the front of the figure.

be an indication of the presence of frustration in the compound. The observed, slightly reduced value of the magnetic saturation moments (≈4.1 μB), compared to the expected value for $3d^5$ cations (5 μB), could also be interpreted in this sense (*8, 35*). Therefore we have to be aware of the fact that the spin arrangement does not necessarily reflect the sign of the coupling. To check the relevance of the determined magnetic structure, the nature of the magnetic coupling in $BaMnFeF_7$ will be discussed in the next section.

5. Discussion

In $BaMnFeF_7$, the magnetic interactions between Mn^{2+} and Fe^{3+} spins take place mainly through two types of superexchange paths:

—a 180°-type path involving bridging fluoride ions of corner-sharing octahedra (Mn^{2+}–F^-–Fe^{3+}),

—a 90°-type path via (two) fluoride bridges of edge-sharing octahedra (Mn^{2+}–F^-–Mn^{2+}).

Assuming that these nearest neighbor interactions are the strongest ones, other possible next nearest neighbor interactions (super-superexchange) will be neglected.

The d^5–d^5 interaction via 180°-type superexchange paths is well documented in the literature (*8, 36–38*) as leading to antiferromagnetic (AF) coupling. The situation is less clear for the 90°-type superexchange path. The Kanamori–Goodenough rules (*36, 37*) emphasize the weakness of this interaction, even to the point that there is some doubt about its sign. From the experimental point of view, very few manganese fluorides are known, where Mn^{2+} ions are located in edge-sharing octahedra and where the sign of coupling constants is known. The two examples provided by MnF_2 and $MnAlF_5$ are very significant. In the former, the coupling constant via the 90° superexchange path has been measured and was found to be ferromagnetic (F) ($J' = +0.325$ K (*39*)). In the latter, the nonfrustrated spin arrangement unambiguously implies an AF coupling (*40, 41*). Some light may be shed on these apparently contradictory results from a careful examination of the local configuration that implies this interaction.

As is well known, the two main geometric parameters governing superexchange coupling are, for given magnetic species, the superexchange angle and the separation between interacting centers (*42*). The fact that an interaction is reinforced when distances are shorter has already been pointed out (*42, 43*), as well as the linear dependence of the coupling constant on the bridge angle β or a function of it like $\cos^2 \beta$ (*42, 44–48*). In a d^5–d^5 superexchange coupling, the strongest AF interaction occurs at $\beta = 180°$. The strength of the interaction decreases with β and the interaction may possibly become ferromagnetic. The problem is to determine the angle β_b for which the transition between AF and F interaction takes place (*46*). Concerning the Mn^{2+}–F–Mn^{2+} exchange, MnF_2 and $MnAlF_5$ provide an answer to this question, as illustrated in Fig. 7. The superexchange angle is about 102° in MnF_2 (*49*) (F interaction) and about 107° in $MnAlF_5$ (*50*) (AF interaction). Thus the magnetic behavior of these compounds becomes consistent with the previous remarks if $102° < \beta_b < 107°$.

The geometry of the superexchange path in $BaMnFeF_7$ is also shown in Fig. 7 (values from Ref. (*21*)). The bridge angle is about 100°, i.e., smaller than in MnF_2, which indicates a tendency toward ferromagnetic coupling, and the shorter Mn–Mn distance should strengthen this interaction compared to MnF_2. Regarding the triangular platelets of the structure (Fig. 8), a ferromagnetic Mn–Mn coupling together with antiferromagnetic Mn–Fe interactions leads to a positive frustration function (*17*), hence to the absence of frustration in the structure. This is at variance from the observed spin reduc-

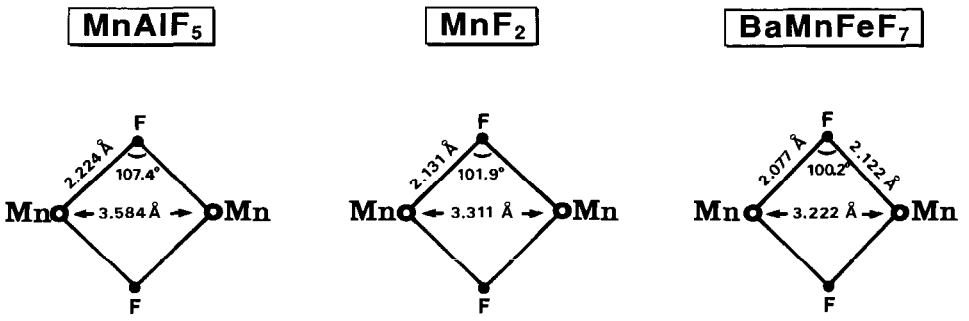

FIG. 7. Geometry of atomic configuration of the superexchange path Mn–F–Mn in $MnAlF_5$ (*50*), MnF_2 (*49*), and $BaMnFeF_7$ (*21*).

tion and from the low temperature magnetic susceptibility behavior, which would have rather suggested the presence of magnetic frustration. On the other hand, direct Mn–Mn exchange might not be negligible in our case (*48*), and it is known to be antiferromagnetic through t_{2g} orbitals. An overall AF Mn–Mn coupling would imply frustration in the triangles, which would better agree with the arguments of spin reduction and the $|\theta_P/T_N|$ value. Once more, the ambiguity on the sign of the coupling constant for the d^5–d^5 90° superexchange path is stressed.

Concerning the spin arrangement in the structure, the respective consequences are

—if $J_{Mn-Mn} > 0$ (F), the spin structure presented above is in perfect accordance with the coupling constants and the magnetic structure is not frustrated;
—if $J_{Mn-Mn} < 0$ (AF), the magnetic structure is frustrated, but the consequence on the spin arrangement is not straightforward, depending on the relative strength of J_{Mn-Mn} and J_{Mn-Fe}.

This second hypothesis, which is the least evident, shall be considered now. It corresponds to the case of a triangular platelet with three AF interactions, $2J$ and $1J'(= J_{Mn-Mn})$. It has been shown (*35*) that over a wide range of negative J' values the presence of frustration does not influence the spin configuration: it remains collinear with a constrained parallel arrangement of the spins which are connected by antiferromagnetic J'. Beyond a certain value J'_{min}, the spin configuration departs from collinearity ($J' < J'_{min} < 0$). For a single platelet $J'_{min} = J/2$. The case of $BaMnFeF_7$ is more difficult to solve analytically than a single isolated platelet, because of the complex magnetic network of the compound. For instance, by looking at the surroundings of the frustrated bond (Fig. 8) one can notice that each direct AF J_{Mn-Fe} coupling is doubled and tripled

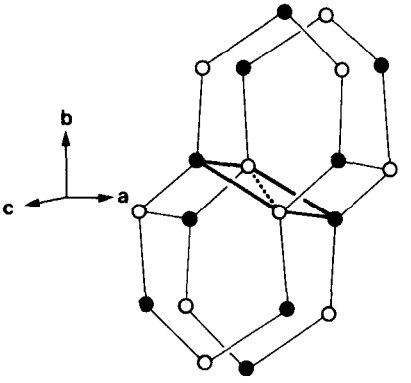

FIG. 8. Cycles of superexchange interactions around the triangular platelets of $BaMnFeF_7$. Open and closed circles represent Mn^{2+} and Fe^{3+} cations, respectively. Solid lines symbolize Mn–F–Fe superexchange interactions (AF) and the dotted line represents Mn–F–Mn interaction, the sign of which determines the presence (AF) or absence (F) of magnetic frustration.

by nonfrustrated AF "indirect" paths (i.e., along square and hexagonal platelets). This strengthens the constraint on the Mn–Mn interaction.

We determined the value of J'_{min} in $BaMnFeF_7$ by Monte Carlo simulation. For this purpose, we used the computer program MCMAG (*51*) which has been designed to simulate the ground-state spin arrangement of any 3-D topology from the values of coupling constants (*52*). The assumption was made, reasonable for d^5 cations, that the single-ion anisotropy is negligible at any magnetic site of the compound. By trial and error, the J'_{min} value could be estimated to about $1.5J$; the spins depart from collinearity for J' of larger magnitude ($J' < 1.5J < 0$). For weaker J' values (recall that J'_{Mn-Mn} is expected to be weaker in magnitude than J_{Mn-Fe}) the result of the simulated spin arrangement was identical with the experimental observation: two sublattices of parallel spins (Mn and Fe spins, respectively) oriented antiparallel to each other.

Thus, even in the second hypothesis and despite the postulated presence of frustration, the magnetic structure of $BaMnFeF_7$ is in very good agreement with what is expected from this kind of exchange interactions in the compound.

6. Conclusion

We have undertaken bulk magnetic measurements and determined the magnetic structure of $BaMnFeF_7$. The results of both methods are consistent with an antiferromagnetic ordering, the sublattices of Mn and Fe remaining ferromagnetically ordered internally. The presence of magnetic frustration in the compound is not clearly evidenced. However, whatever the assumption regarding the sign of the coupling constant J_{Mn-Mn} may be, the magnetic structure determined by neutron diffraction is in good agreement with what is commonly known about d^5–d^5 superexchange interactions in insulators.

Acknowledgment

We are indebted to Professor Gary Long for useful information on his high field Mössbauer measurements of $BaMnFeF_7$.

References

1. G. Ferey, R. De Pape, and B. Boucher, *Acta Crystallogr. B* **34,** 1084 (1978).
2. M. Leblanc, G. Ferey, Y. Calage, and R. De Pape, *J. Solid State Chem.* **53,** 360 (1984).
3. G. Ferey, M. Leblanc, R. De Pape, and J. Pannetier, *Solid State Commun.* **53,** 559 (1985).
4. Y. Laligant, M. Leblanc, J. Pannetier, and G. Ferey, *J. Phys. C Solid State Phys.* **19,** 1081 (1986).
5. M. Leblanc, R. De Pape, G. Ferey, and J. Pannetier, *Solid State Commun.***58,** 171 (1986).
6. Y. Laligant, J. Pannetier, and G. Ferey, *J. Solid State Chem.* **66,** 242 (1987).
7. Y. Laligant, Y. Calage, G. Heger, J. Pannetier, and G. Ferey, *J. Solid State Chem.* **78,** 66 (1989).
8. G. Ferey, R. De Pape, M. Leblanc, and J. Pannetier, *Rev. Chim. Minér.* **23,** 474 (1986).
9. P. Lacorre, J. Pannetier, and G. Ferey, *J. Magn. Magn. Mater.* **66,** 213 (1987).
10. P. Lacorre, M. Leblanc, J. Pannetier, and G. Ferey, *J. Magn. Magn. Mater.* **66,** 219 (1987).
11. Y. Laligant, G. Ferey, G. Heger, and J. Pannetier, *Z. Anorg. Allg. Chem.* **553,** 163 (1987).
12. M. Leblanc, G. Ferey, P. Lacorre, and J. Pannetier, *J. Magn. Magn. Mater.* **92,** 359 (1991).
13. P. Lacorre, J. Pannetier, M. Leblanc, and G. Ferey, *J. Magn. Magn. Mater.* **92,** 366 (1991).
14. P. Lacorre, J. Pannetier, and G. Ferey, *J. Magn. Magn. Mater.* **94,** 331 (1991).
15. P. Lacorre, M. Leblanc, J. Pannetier, and G. Ferey, *J. Magn. Magn. Mater.* **94,** 337 (1991).
16. P. Lacorre, J. Pannetier, T. Fleischer, R. Hoppe, and G. Ferey, *J. Solid State Chem.* **93,** 37 (1991).
17. G. Toulouse, *Commun. Phys.* **2,** 115 (1977).
18. J. Vannimenus and G. Toulouse, *J. Phys. C Solid State Phys.* **10,** L537 (1977).
19. M. Samouël and A. de Kozak, *Rev. Chim. Minér.* **15,** 268 (1978).
20. A. de Kozak and M. Samouël, *Rev. Chim. Minér.* **15,** 406 (1978).

21. H. HOLLER, D. BABEL, M. SAMOUËL, AND A. DE KOZAK, *J. Solid State Chem.* **39,** 345 (1981).
22. H. M. RIETVELD, *J. Appl. Crystallogr.* **2,** 65 (1969).
23. A. W. HEWAT, Harwell Report AERE-R 7370 (1973).
24. L. KOESTER AND H. RAUCH, "Summary of Neutron Scattering Lengths," IAEA Contract 2517/RB (1981).
25. R. E. WATSON AND J. FREEMAN, *Acta Crystallogr.* **14,** 27 (1961).
26. E. F. BERTAUT, *in* "Magnetism" (G. T. Rado and H. Suhl, Eds.), Vol. III, p. 149, Academic Press, New York (1963).
27. J. PEBLER AND F. W. RICHTER, *Z. Phys.* **221,** 480 (1969).
28. G. K. WERTHEIM, H. J. GUGGENHEIM, AND D. N. E. BUCHANAN, *Phys. Rev.* **169,** 465 (1968).
29. G. LONG, private communication (1984).
30. A. TRESSAUD AND J. M. DANCE, *in* "Structure and Bonding," Vol. 52, p. 87, Springer-Verlag, New York/Berlin (1982).
31. J. PEBLER, K. SCHMIDT, D. BABEL, AND W. VERSCHAREN, *Z. Naturforsch. B* **32,** 369 (1977).
32. S. NAGEL, *Phys. Rev. B* **24,** 4240 (1981).
33. S. NAGEL, *J. Chem. Phys.* **46,** 905 (1985).
34. J. M. D. COEY, *Can. J. Phys.* **65,** 1210 (1987).
35. P. LACORRE, *J. Phys. C Solid State Phys.* **20,** L775 (1987).
36. L. KANAMORI, *J. Phys. Chem. Solids* **10,** 87 (1959).
37. J. B. GOODENOUGH, "Magnetism and the Chemical Bond" (F. A. Cotton, Ed.), Wiley–Interscience, New York (1963).
38. L. J. DE JONGH AND R. BLOCK, *Physica B* **79,** 568 (1975).
39. O. NIKOTIN, P. A. LINGDÅRD, AND O. W. DIETRICH, *J. Phys. C Solid State Phys.* **2,** 1168 (1969).
40. A. TRESSAUD, J. M. PARENTEAU, J. M. DANCE, J. PORTIER, AND P. HAGENMULLER, *Mater. Res. Bull.* **8,** 565 (1973).
41. M. WINTENBERGER, J. M. DANCE, AND A. TRESSAUD, *Solid State Commun.* **17,** 185 (1975).
42. H. J. ZEIGLER AND G. W. PRATT, *in* "Magnetic Interactions in Solids," p. 244, Clarendon Press, Oxford (1973).
43. K. N. SHRIVASTAVA, *Phys. Status Solidi B* **125,** 11 (1984).
44. C. BOEKEMA, F. VAN DER WOUDE, AND G. A. SAWATZSKY, *Int. J. Magn.* **3,** 341 (1972).
45. G. A. SAWATZKY AND F. VAN DER WOUDE, *J. Phys. Paris* **12,**C6-47 (1974).
46. K. N. SHRIVASTAVA, *Phys. Status Solidi B* **125,** 441 (1984).
47. J. PEBLER, W. MASSA, H. LASS, AND B. ZIEGLER, *J. Solid State Chem.* **71,** 87 (1987).
48. K. MOTIDA AND S. MIYAHARA, *J. Phys. Soc. Jpn.* **28,** 1188 (1970).
49. W. H. BAUR AND A. A. KHAN, *Acta Crystallogr. B* **27,** 2133 (1971).
50. G. FEREY, *J. Solid State Chem.*, in press.
51. P. LACORRE, I.L.L. Technical Report 88LA13T (1988).
52. P. LACORRE AND J. PANNETIER, *J. Magn. Magn. Mater.* **71,** 63 (1987).